

Anionic redox reaction mechanism in Na-ion batteries

Xueyan Hou(侯雪妍), Xiaohui Rong(容晓晖), Yaxiang Lu(陆雅翔), and Yong-Sheng Hu(胡勇胜)
Citation: Chin. Phys. B, 2022, 31 (**9**): 098801. DOI: 10.1088/1674-1056/ac81ab
Journal homepage: http://cpb.iphy.ac.cn; http://iopscience.iop.org/cpb

What follows is a list of articles you may be interested in

Charge transfer modification of inverted planar perovskite solar cells by NiO_x/Sr:NiO_x bilayer hole transport layer

Qiaopeng Cui(崔翘鹏), Liang Zhao(赵亮), Xuewen Sun(孙学文), Qiannan Yao(姚倩楠), Sheng Huang(黄胜), Lei Zhu(朱磊), Yulong Zhao(赵宇龙), Jian Song(宋健), and Yinghuai Qiang(强颖怀)
Chin. Phys. B, 2022, 31 (**3**): 038801. DOI: 10.1088/1674-1056/ac1fda

Pair distribution function analysis: Fundamentals and application to battery materials

Xuelong Wang(王雪龙), Sha Tan(谭莎), Xiao-Qing Yang(杨晓青), Enyuan Hu(胡恩源)
Chin. Phys. B, 2020, 29 (**2**): 028802. DOI: 10.1088/1674-1056/ab6656

Advanced characterization and calculation methods for rechargeable battery materials in multiple scales

Xin-Yan Li(李欣岩), Su-Ting Weng(翁素婷), Lin Gu(谷林)
Chin. Phys. B, 2020, 29 (**2**): 028801. DOI: 10.1088/1674-1056/ab65ba

High capacity sodium-rich layered oxide cathode for sodium-ion batteries

Gen-Cai Guo(郭根材), Changhao Wang(王长昊), Bang-Ming Ming(明帮铭), Si-Wei Luo(罗斯玮), Heng Su(苏恒), Bo-Ya Wang(王博亚), Ming Zhang(张铭), Hai-Jun Yu(尉海军), Ru-Zhi Wang(王如志)
Chin. Phys. B, 2018, 27 (**11**): 118801. DOI: 10.1088/1674-1056/27/11/118801

All-solid-state lithium batteries with inorganic solid electrolytes: Review of fundamental science

Xiayin Yao(姚霞银), Bingxin Huang(黄冰心), Jingyun Yin(尹景云), Gang Peng(彭刚), Zhen Huang(黄祯), Chao Gao(高超), Deng Liu(刘登), Xiaoxiong Xu(许晓雄)
Chin. Phys. B, 2016, 25 (**1**): 018802. DOI: 10.1088/1674-1056/25/1/018802

TOPICAL REVIEW — Celebrating 30 Years of *Chinese Physics B*

Anionic redox reaction mechanism in Na-ion batteries

Xueyan Hou(侯雪妍)[1], Xiaohui Rong(容晓晖)[1,†], Yaxiang Lu(陆雅翔)[1], and Yong-Sheng Hu(胡勇胜)[1,2,‡]

[1] *Key Laboratory for Renewable Energy, Beijing Key Laboratory for New Energy Materials and Devices, Beijing National Laboratory for Condensed Matter Physics, Institute of Physics, Chinese Academy of Sciences, Beijing* 100190, *China*

[2] *Center of Materials Science and Optoelectronics Engineering, University of Chinese Academy of Sciences, Beijing* 100190, *China*

(Received 23 April 2022; revised manuscript received 12 July 2022; accepted manuscript online 18 July 2022)

Na-ion batteries (NIBs), as one of the next-generation rechargeable battery systems, hold great potential in large-scale energy storage applications owing to the abundance and costeffectiveness of sodium resources. Despite the extensive exploration of electrode materials, the relatively low attainable capacity of NIBs hinders their practical application. In recent years, the anionic redox reaction (ARR) in NIBs has been emerging as a new paradigm to deliver extra capacity and thus offers an opportunity to break through the intrinsic energy density limit. In this review, the fundamental investigation of the ARR mechanism and the latest exploration of cathode materials are summarized, in order to highlight the significance of reversible anionic redox and suggest prospective developing directions.

Keywords: energy storage, Na-ion battery, anionic redox reaction

PACS: 88.80.ff, 82.47.Aa, 71.20.–b, 68.55.Nq **DOI:** 10.1088/1674-1056/ac81ab

1. Introduction

Confronting the pressing energy and environmental challenges, energy storage technology is crucial in the ongoing electrification process. As the most successful rechargeable battery, Li-ion batteries (LIBs) have been powering portable electronics for decades and hold great potential in the emerging electric vehicle market. However, the large-scale utilization is limited by the scarcity and high cost of lithium. Na-ion batteries (NIBs), promising candidates to supplement current energy storage technologies, have been extensively investigated due to the abundance and accessibility of sodium in recent years.[1–5] The cathode material is the crucial component in determining the electrochemical performance of cells, including operating voltage and specific capacity. Layered transition metal oxides, polyanion compounds, Prussian blue analogues are applicable NIB cathode materials, and among which layered transition metal oxides are considered the most promising candidates and have received extensive investigation.[6–12] Delmas *et al*.[13] classified the crystal structure of layered transition metal oxides by the coordination environment of alkali metal ions as shown in Fig. 1(a): "O" and "P" represent the octahedral and prismatic coordination, respectively, and "2" or "3" represent the number of alkali layers in a unit cell. The conventional LIB transition metal oxide cathodes, *e.g.* $LiCoO_2$, are indexed with O3-type structures, while the layered structure of NIB oxide cathodes is more complex and diverse in TM component and structure, which can be categorized into O2, O3, P2, and P3 types.[14–16]

Although NIBs work on a similar principle as LIBs, *i.e.*, intercalation chemistry of alkali metal ions (A^+), their practical application is hindered by the relatively low gravimetric/volumetric energy density because Na^+ is heavier and larger than Li^+. In this context, the research of anionic redox reaction (ARR) of Li excess cathodes is an inspiration because the research in LIBs suggests that it provides extra capacity, thus enabling higher energy density than conventional cationic redox reaction. Conceivably, anionic redox offers an opportunity for the development of high-energy-density NIBs.[17–19] In this review, we briefly outline the fundamental studies of the underlying reaction mechanism, the progress of the anionic redox-based NIB cathode materials, and the challenges hindering practical applications, from which we highlight the significance of reversible anionic redox and suggest prospective developing directions.

2. Fundamental of anionic redox reaction

The discovery of charge compensation by oxygen redox in Li_2MnO_3 (or $Li(Li_{1/3}Mn_{2/3})O_2$) preludes the extensive investigation of anionic redox chemistry in LIBs,[20,21] after which several Li-excess cathode materials, *e.g.*, $Li_{1.2}Ni_{0.2}Mn_{0.6}O_2$ and $Li_{1.2}Ni_{0.13}Co_{0.13}Mn_{0.54}O_2$, also deemed solid solutions of layered $LiTMO_2$ and Li_2MnO_3, were reported to deliver extra capacity by anionic redox.[22] The typical voltage profiles (*versus* state of charge) of the classical layered cathode $LiCoO_2$ and Li-excess cathode $Li_{1.2}Ni_{0.2}Mn_{0.6}O_2$ are compared, as depicted in Fig. 1(b). During charging and discharging, the charge neutrality by Li extraction/insertion is balanced by TM redox in the conven-

†Corresponding author. E-mail: rong@iphy.ac.cn
‡Corresponding author. E-mail: yshu@iphy.ac.cn

© 2022 Chinese Physical Society and IOP Publishing Ltd

tional layered cathode. In Li-excess cathodes, the oxidation of stable Mn^{4+} has not been experimentally verified during delithiation, while oxygen participates in the redox process at a high voltage which provides partially reversible capacity during cycling. The fundamentals underlying reversible anionic redox have been widely investigated by theoretical studies in recent years. As illustrated in Fig. 2(a), oxygen ions are coordinated with 3 Li ions in the Li layer and 3 TM ions in the TM layer in the structure of ideal Li-stoichiometric $LiTMO_2$ where TM ions are octahedrally coordinated with 6 oxygen atoms; O 2p orbitals hybridize with the TM orbitals along the linear Li–O–M configuration, forming σ-type bonds.[23] The linear combination of TM outer p, d, and s orbitals and O 2p orbitals generates bonding molecular orbitals (MO) at a lower energy level and antibonding molecular orbitals (MO^*) at a higher energy level (Fig. 2(b)).[19] For 3d transition metal oxides, the bonding e_g^b and anti-bonding e_g^* states arise from the overlap between TM $d_{x^2-y^2}$, d_{z^2} and O 2p orbitals; the bonding a_{1g}^b and antibonding a_{1g}^* states are generated from overlap between TM 4s and O 2p orbitals; the bonding t_{1u}^b and antibonding t_{1u}^* states stem from the overlap between TM 4p and O 2p orbitals; the overlap between the TM d_{xy}, d_{yz}, and d_{xz} orbitals form t_{2g} states. The antibonding e_g^*, a_{1g}^*, t_{1u}^*, and t_{2g} states have dominating TM character, while the bonding e_g^b, a_{1g}^b, and t_{1u}^b states have dominating O character.[24] The electrons in the MO^* states reversibly participate in the redox activity by charging and discharging. With more than half of the Li extraction from $LiCoO_2$, irreversible lattice oxygen loss was observed, which can be ascribed to the formation of holes in the O 2p state.[25] Researchers generally accept that such an anionic oxidation process in charging is essentially irreversible and leads to electrochemical degradation, so that the intrinsic voltage limit is determined by the energy of the O 2p state. In Li-excess cathodes, 1/3 of the TM sites are occupied by A ions in the Li_2MnO_3 phase, forming a so-called honeycomb structure.[26] Seo *et al.*[23] demonstrated that the oxygen 2p orbitals are unhybridized (orphaned) in the direction of the Li–O–Li configuration owing to the large energy difference between the Li 2s and O 2p states as depicted in Fig. 2(c). The non-bonding O 2p state participates in the redox and provides extra reversible capacity, the energy of which is located below antibonding orbitals and on the top of bonding orbitals (Fig. 2(d)). The nature of oxidized oxygen by anionic redox during cycling is another crucial issue. Irreversible capacity loss has been widely reported in the initial charging process as depicted in Fig. 1(b). $(O_2)^{n-}$ species and even molecular oxygen are formed in the first de-lithiation, leading to irreversible reorganization of the oxygen network and cation migration to stabilize the formation of O–O bonds; after the initial charging, $(O_2)^{n-}$ species reversibly participate in the subsequent cycling process.[27,28]

To theoretically elucidate the reversibility of anionic redox, researchers introduced the Mott–Hubbard theory: the partially filled MO^* band is split into a fully-filled lower-Hubbard band (LHB) and an empty upper-Hubbard band (UHB), as illustrated in Figs. 2(e)–2(g).[19,29] The d–d Coulomb interaction term U is the energy gap between LHB and UHB that increases from the left to right in the periodic table and decreases from 3d to 5d transition metals. The charge transfer term Δ represents the energy difference between bonding MO and antibonding MO^*, determined by the electronegative difference between the metal and anion ligand. The reversibility of anionic redox depends on the interplay between U and Δ. For the situation $U \ll \Delta$, electrons in fully-filled LHB participate in the redox as in classical cationic redox. For $U/2 \approx \Delta$, the LHB overlaps with the non-bonding O 2p state, leading to reversible cationic and anionic redox and MO_6 distortion and O–O shortening. For $U \gg \Delta$, electrons are directly removed from the non-bonding O 2p state located above the filled LHB, resulting in reactive $(O_2)^{n-}$ species and irreversible oxygen loss. From the discussion in terms of the σ-type hybridization, we summarize the prerequisite of reversible anionic redox for intercalation oxide cathodes: (i) the formation of oxygen lone pairs and associated non-bonding O 2p states and (ii) rational modulation of the U and Δ terms of the material ($U/2 \approx \Delta$).

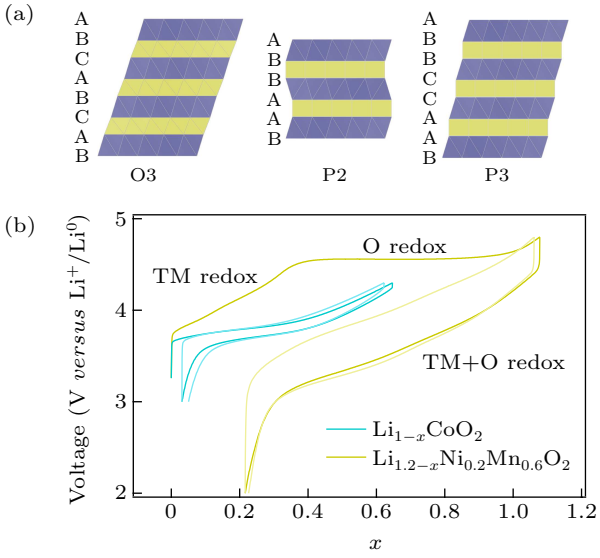


Fig. 1. (a) Illustration of the O3-, P2-, and P3-type crystal structures of NIB cathodes exhibiting ARR, the oxygen of which has ABCABC, ABBA, and ABBCCA stacking, respectively. (b) Comparison of conventional layered oxide cathodes and A-excess oxide cathodes: typical voltage *versus* state of charge profiles of cells with conventional $LiCoO_2$ cathode (blue) and Li-excess $Li_{1.2}Ni_{0.2}Mn_{0.6}O_2$ cathode (yellow). The light color denotes the performances of the 2nd cycle.

On the other hand, the metal-ligand π-type interaction has attracted wide attention in recent years, which was predicted to play a key role in anionic redox reaction.[30] As has been stated, the σ-type overlap between TM d_{xy}, d_{yz}, and d_{xz} orbitals (t_{2g} states) and O 2p orbitals has been considered

negligible.[23] However, Sudayama *et al.*[31] demonstrated the presence of π-type interaction between TM t_{2g} orbitals with O 2p orbital. From the conventional perspective, TM and O usually form σ bond with the σ donation from oxygen, the 2p orbitals of which are fully filled; by O oxidation, instable holes are formed in the O 2p orbitals and stabilized by π back-donation from TM, termed as the $(\sigma+\pi)$ multiorbital bonds. Tsuchimoto *et al.*[32] experimentally studied the nonpolarizing oxygen redox in $Na_2Mn_3O_7$ and verified that the formation of $(\sigma+\pi)$ multiorbital bond stabilizes the O 2p holes thus leads to better reversibility of ARR. Kitchaev *et al.*[33] also demonstrated that the nonhysteretic excess capacity in $Na_2Mn_3O_7$ and Li_2IrO_3 is a result of a network of π-bonded TM d and O 2p orbitals, TM migration is mitigated by which as well. Song *et al.*[34] also reported the Li–O–Li axis indeed has π-type interaction with Mn t_{2g} states in Li-excess cathode, which can account for the fact that the number and type of neighboring TM species significantly influence the ARR performance. Zhang *et al.*[35] suggested that the π-type metal-ligand interaction can trigger a new low-voltage oxygen redox activity, which is distinct from the above-stated high-voltage oxygen redox reaction of the nonbonding O 2p state. Although the recent inspiring advances of the fundamental knowledge offer new perspectives of the anionic redox reaction mechanism, more experimental researches in atomic level is highly desired for in-depth understanding and validated this concept in more SIB anionic redox cathode materials with diverse TM composition and structure. In a word, investigating the fundamental mechanism underlying ARR can provide critical insights for researchers to explore strategies of designing and modifying ARR cathode materials.

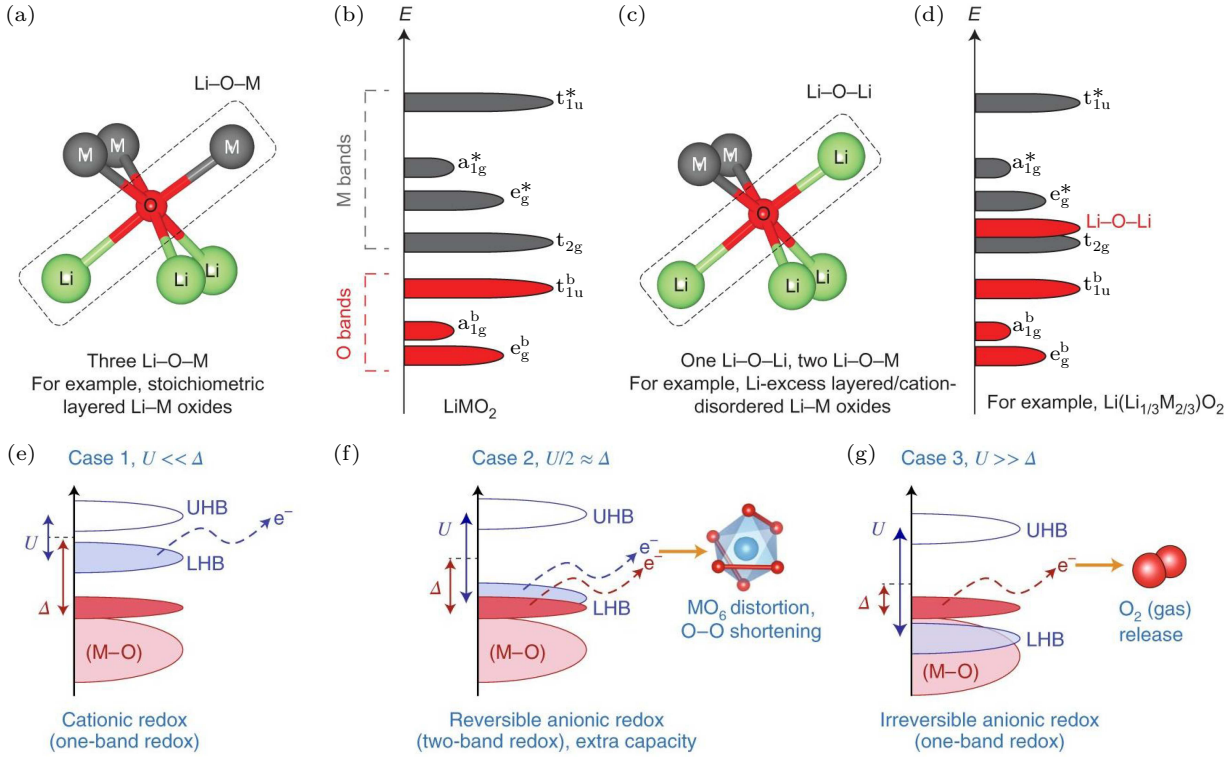


Fig. 2. (a) Local coordination environment of oxygen consisting 3 Li–O–TM configurations and (b) the schematic diagram of the band structure in Li-stoichiometric $LiTMO_2$. (c) The local coordination environment of oxygen consisting one Li–O–Li and two Li–O–TM configurations and (d) the schematic diagram of the band structure in the Li-excess Li_2MnO_3. Reproduced with the permission from Ref. [23]. Copyright ©2016, Nature Publishing Group. Schematic diagram of the band structure in Li_2MnO_3 considering the Mott-Hubbard splitting in the condition of (e) $U \ll \Delta$, (f) $U/2 \approx \Delta$, and (g) $U \gg \Delta$. Reproduced with the permission from Ref. [19]. Copyright ©2018, Nature Publishing Group.

3. Progresses of anionic redox based NIB cathodes

Inspired by studies in LIBs, the as-described anionic redox has emerged as a promising paradigm to break through the intrinsic energy density limit of NIBs. Figure 3 summarizes the average discharge voltage (*versus* Na^+/Na^0) and attainable capacity of several NIB cathodes based on pure cationic redox and pure anionic redox or cumulative cationic and anionic redox; the latter is significantly advantageous in raising the battery's energy density and even drawing near the performance of LIBs. Although the NIBs work on the same intercalation principle as the LIBs, the counterparts of the two systems are not exactly comparable. As has been stated in terms of the classification of layered oxides, layered cathodes for LIBs (including Li-excess materials) usually have O3-type structures where "O" and "3" represent the octahedral coordination environment of alkali metal ions and the ABCABC

stacking, respectively.[13] Different from the Li counterpart, the crystal structure of anionic redox NIB cathodes is more diverse. Sodium oxide cathodes exhibiting anionic redox can be synthesized in different structures, including not only the O3-type but also the P2 and P3 structures (Fig. 1(a)), where "P" indicates the prismatic coordination environment of the alkali metal ion, and "2" and "3" indicate the ABBA and ABBCCA oxygen stacking, respectively.

A-rich compounds with the general formula $A[A_xTM_{1-x}]O_2$ ($x \neq 0$) are widely accepted as ARR cathodes, including A_2TMO_3 isostructural with Li_2MnO_3, as well as A_5TMO_6, *etc*. The anionic redox reaction in such materials can be interpreted by the above-stated A–O–A configuration (Li–O–Li or Na–O–Na), along which the nonbonding O 2p state is formed. Deduced from the universal octet rule, four electron pairs are needed in the oxygen valence shell for stabilization. The x stoichiometry of $A[A_xTM_{1-x}]O_2$ is directly related to the number of oxygen lone pairs. For typical compositions $ATMO_2$ ($x = 0$), A_2TMO_3 ($x = 1/3$) and A_5TMO_6 ($x = 2/3$) with order cationic arrangement, the average coordination numbers of TM around O are 3, 2, and 1, respectively, leading to 0, 1, and 2 oxygen lone pairs per oxygen in unit structure. Yahia *et al.*[29] applied the term, number of holes per oxygen (h^O), to quantify the reversibility of anionic redox reaction and suggested that $h^O = 1/3$ is the critical value to avoid irreversible lattice oxygen release. The charge transfer term can also determine the number of holes. In this regard, to minimize the irreversibility of ARR and optimize the battery energy density, cumulative cationic redox capacity and anionic redox capacity are limited to $h^O \leq 1/3$. As for Na-excess compounds, only limited O3-type cathodes are reported to exhibit ARR, mainly 4d and 5d TM-based materials including Na_2RuO_3,[48,49] Na_2IrO_3,[50] and derivatives, *e.g.*, $Na_2Ru_{1-y}Sn_yO_3$,[51] and $Na_{1.2}Mn_{0.4}Ir_{0.4}O_2$.[52] Although the strong covalency of Ru–O and Ir–O bonding enables highly stable anionic redox, the practical application of 4d and 5d TM-based cathodes is hindered by their high cost and low abundance. However, the Li_2MnO_3 counterpart Na_2MnO_3 material is hard to obtain owing to the large size mismatch between Mn^{4+} ($r = 0.53$ Å) and Na^+ ($r = 1.02$ Å).

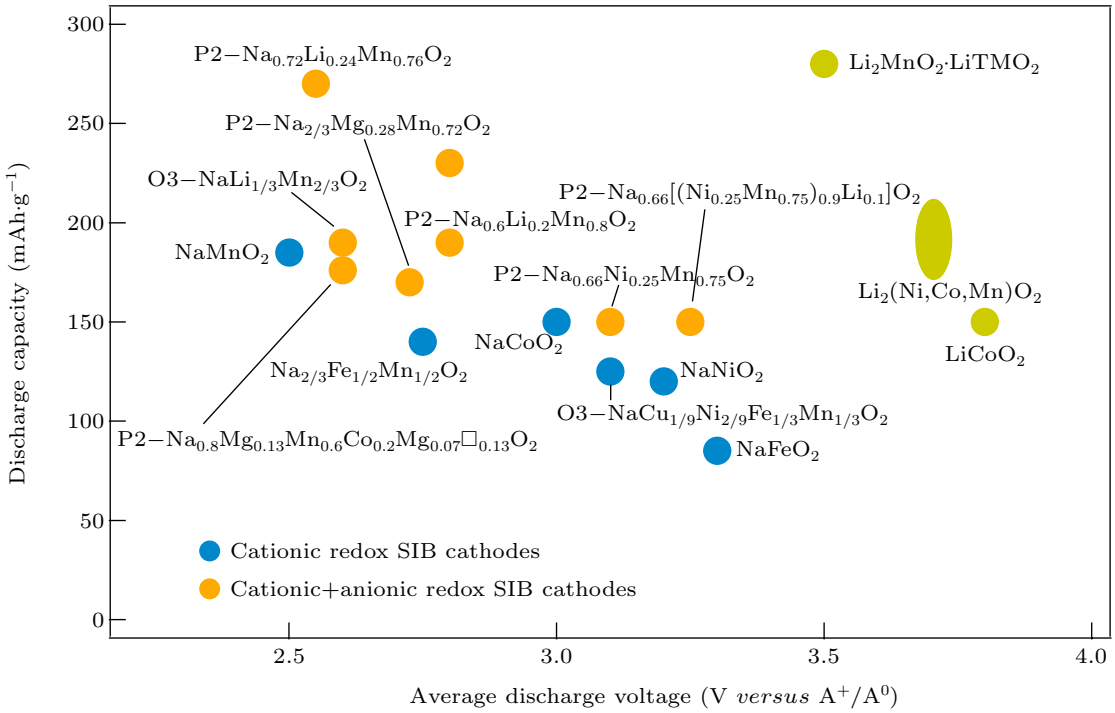


Fig. 3. Comparison of the specific discharge capacity and average discharge voltage (*versus* Na^+/Na^0) of reported oxide-based NIB cathode materials based on different redox mechanisms.[36–47] The performance of layered and Li-excess oxide cathodes for LIBs (with Li metal as the counter and reference electrodes) are also displayed as references.

The term TM/O is utilized by Zhao *et al.*[53] to characterize the ARR performance since it is directly related to the oxygen coordination environment; figure 4 illustrates the structural evolution of ARR electrodes with different TM/O ratios, in which the A-excess compounds are listed. However, the unexpected region in $1/2 < TM < 1/3$ marked in violet represents the important NIB cathodes exhibiting ARR in addition to A-excess compounds, namely the Na-deficient phase. In this case, it should be noted that the specific discharge capacity of Na-deficent cathodes can be higher than the charge capacity owing to the extra Na^+ intercalation after the first charging process, accompanied with the reduction of Mn^{4+} to Mn^{3+} as charge compensation mechanism at low operating voltage.[7,17,54]

As one of the distinguishing features of anionic redox-based NIBs, Na-stoichiometric and many Na-deficient 3d TM-

based cathode materials were reported to show reversible anionic redox activity, *e.g.*, O3-$NaLi_{1/3}Ti_{1/6}Mn_{1/2}O_2$,[36] P2-$Na_{2/3}Ni_{1/3}Mn_{2/3}O_2$,[55,56] P3-$Na_{0.6}Li_{0.2}Mn_{0.6}O_2$,[57] and the hybrid P–O system $Na_2Mn_3O_7$ (or $Na_{4/7}Mn_{6/7}\square_{1/7}O_2$, $\square$ denotes vacancy).[32,58] Anionic redox cathodes have exhibited other interesting features in addition to their high specific capacity. Rong *et al.*[59] reported the high structural and reaction stability of P3-$Na_{0.6}[Li_{0.2}Mn_{0.8}]O_2$ owing to the immobile nature of cations in the TM layer and stabilized O–O dimer. ARR in P2-$Na_{0.72}[Li_{0.24}Mn_{0.76}]O_2$ was reported to stabilize the structure of P2-$Na_{0.72}[Li_{0.24}Mn_{0.76}]O_2$ in desodiation by suppressing the P2–O2 phase transition and mitigating volume change as a result of the reduced Coulombic repulsion of oxygen layers.[41] $Na_2Mn_3O_7$ displayed rather low voltage hysteresis compared with Li-excess cathodes, which was attributed to the hole stabilization.[32,60] P2-$Na_{2/3}Ni_{1/3}Mn_{2/3}O_2$, whose charge compensation mechanism was once controversial, exhibited superior air stability and electrochemical reversibility with a strong ARR.[61,62]

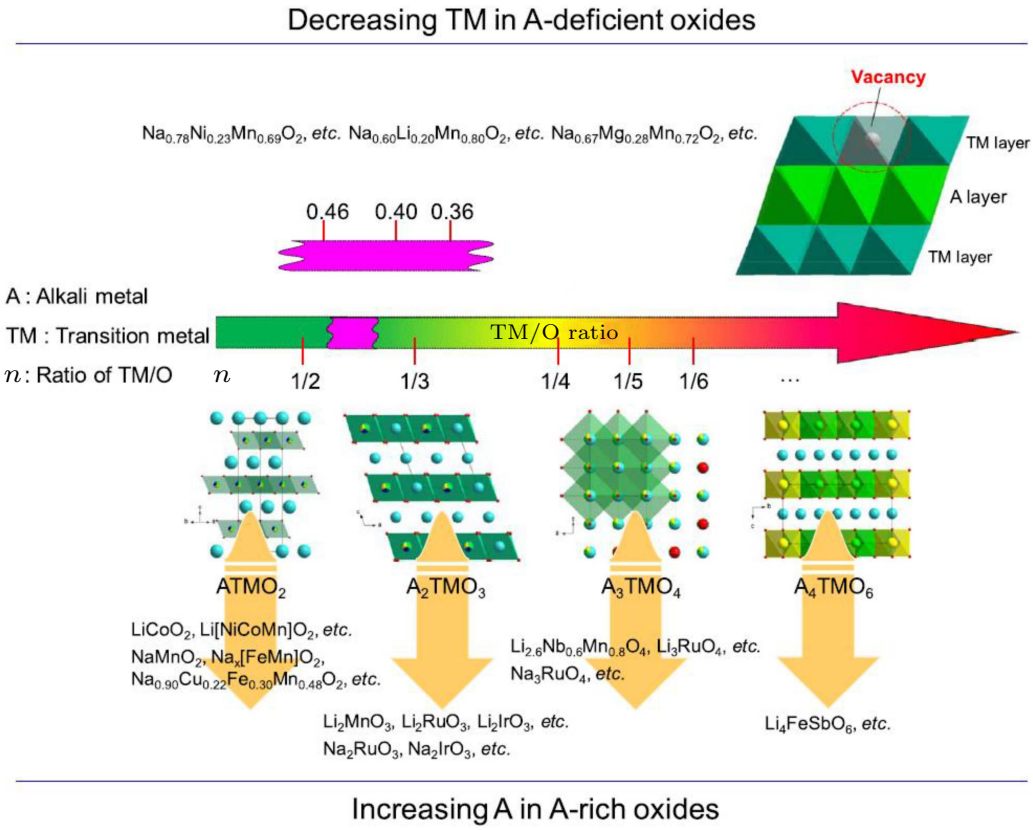


Fig. 4. Structural illustration of reported ARR electrodes with different TM/O ratios. Reproduced with the permission from Ref. [53]. Copyright ©2018, Elsevier B.V.

In these Mn-based NIB cathodes, cation mixing between the Na and TM layers is unfavorable owing to the size mismatch between Na^+ and Mn^{4+}, so the Na–O–Na configuration is unlikely to exist as the Li–O–Li configuration in the cation disordered LIB cathode. In the absence of the Na–O–Na or Li–O–Li configuration, the underlying mechanism of anionic redox in the Na-deficient/stoichiometric materials is an intriguing problem. As has been widely reported, substitution of electrochemically inactive species for TM is an effective method to generate oxygen lone pairs and the non-bonding O 2p state. Li, inactive d^0 metal species (*e.g.*, Mg ($3s^2$) and Zn ($4s^2$), to be referred to as M′), and $\square$ (vacancy) are widely reported electrochemically inactive species to form Na–O–Li, Na–O–M′, Na–O–$\square$, $\square$–O–Li, $\square$–O–M′, and $\square$–O–$\square$ configurations that generate the non-bonding O 2p state.[37,40,53,65] Additionally, the Mg–O–Mg configuration was also reported to be formed by introducing Mg^{2+} in both Na and TM layers, promoting reversible oxygen redox.[66] Figure 5(a) summarizes the possible configurations contributing to anionic redox. In this regard, the design and tailoring of anionic redox cathode materials for NIBs are much more flexible and diverse than those for LIBs. On the other hand, the reversibility of lattice oxygen redox is another intriguing problem that is highly related to electrochemical performance. Studies in recent years have demonstrated the critical role of the TM layer ordering or superstructure in anionic redox reversibility. For instance, de Boisse *et al.*[49] revealed that the honeycomb cation ordering in Na_2RuO_3 is a structural requisite condition for stable oxygen redox reactions. House *et al.*[63] exhibited the effect of Li–Mn ordering in the TM layer (Fig. 5(b)) and

determined the first-cycle voltage hysteresis: the honeycomb ordering in $Na_{0.75}[Li_{0.25}Mn_{0.75}]O_2$ was disrupted by the in-plane Mn migration that induced O_2 formation in charging and changed the local coordination of O^{2-} in discharging, while the ribbon superstructure in $Na_{0.6}[Li_{0.2}Mn_{0.8}]O_2$ inhibited Mn migration and suppressed O_2 formation and stabilized electron holes on O^{2-}. Furthermore, Gao *et al.*[64] investigated the stacking features in P2- and P3-$Na_{0.6}Li_{0.2}Mn_{0.8}O_2$ with ribbon superstructure and revealed the key role of topological protection provided by the $-\alpha-\gamma-$ stacking in enhancing the anionic redox reversibility. In short, the structural and chemical versatility offers vast possibilities in the exploration of anionic redox based oxide cathodes for NIBs.

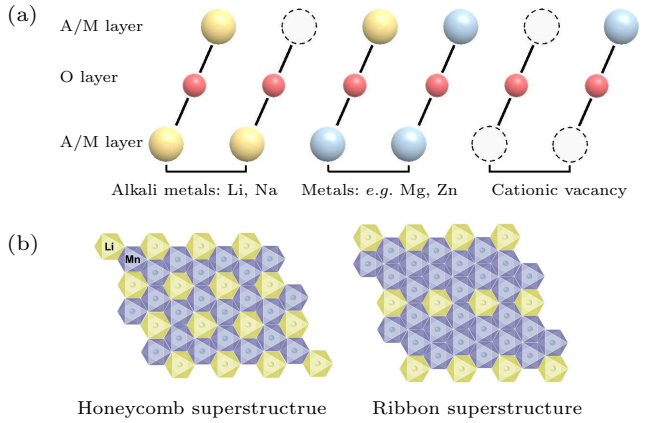


Fig. 5. (a) Schematic illustration of the possible configuration generating oxygen lone pairs in NIB cathodes. (b) Illustration of Li/Mn ordering in the TM layer in the Mn-based NIB cathode: honeycomb superstructure (left) and ribbon superstructure (right).[63,64]

Despite the high capacity and energy density enabled by anionic redox, some issues, *e.g.*, capacity fade and voltage hysteresis hinder their practical application.[67] Electrochemical degradation is related to irreversible lattice oxygen release and structural transformation induced by lattice reorganization cation migration.[27,28] On the other hand, exothermic side reactions take place between the released molecular oxygen with the organic electrolyte and electrode materials, which generates more gas species and leads to safety hazards. In-depth investigation of the irreversible anionic redox reaction and the degradation mechanism is desired to build a robust NIB with a high energy density. The development of advanced characterization techniques has promoted intensive research in recent years, especially the emerging synchrotron-based techniques and in-situ operations.[68] For the oxygen redox activity, "conventional" x-ray photoelectron spectroscopy (XPS) and x-ray absorption spectroscopy (XAS) have been widely employed to characterize the electronic structure of materials. The XPS is, however, surface sensitive, while the XAS is both surface (electron yield) and bulk sensitive (fluorescence yield). *In-situ* and *ex-situ* soft XAS (sXAS) technique has been widely applied to analyse the in-depth mechanism of oxygen activities, especially the redox of oxygen species, by characterizing O *K*-edge spectra. Despite that, the pre-peak of O *K*-edge soft XAS essentially reflects the hybridization of TM 3d and O 2p states with dominating TM 3d character.[69,70] In this context, resonant inelastic x-ray scattering (RIXS) has emerged as a powerful and reliable tool for analyzing oxygen redox activity, which can distinguish the oxidized oxygen state from TM 3d character.[61,71] In terms of the oxygen redox byproducts, the O–O species can be detected by the electron paramagnetic resonance (EPR) and the Raman spectroscopy, which are sensitive to the O–O vibrations;[72,73] *in-situ* DEMS can effectively monitor the gas generation during cycling, including the irreversible lattice oxygen release.[74] For structure characterization, more sophisticated information (*e.g.*, local ordering) can be provided from methods beyond the "conventional" laboratory x-ray diffraction (XRD), including synchrotron XRD and neutron diffraction;[75,76] the pair distribution function (PDF) from neutron total scattering enables direct detection of the interlayer O–O distance and TM–O bond length.[50,59,71,77,78]

4. Conclusion and perspectives

As a promising rechargeable battery system, NIBs offer sustainability and diversity for the energy storage technologies, especially on a large-scale application due to the natural abundance and low cost of sodium (Fig. 6); however, they suffer from intrinsic limited energy density. The anionic redox reaction (ARR) is an emerging paradigm of NIBs that provides extra capacity beyond cationic redox and enhances the operating voltage. In this review, we briefly outlined the latest research progress on NIB cathodes based on ARR, including fundamental studies and material exploration. ARR-based NIB cathode materials exhibit structural and chemical versatility, which enables diversity and flexibility in exploring and designing new materials. Considering the large-scale application scenarios for NIBs, 3d TM-based compounds are conceivably the preferred choice from a practical point of view, while the scarcity and expense of 4d/5d TM elements will undermine the significant advantages of NIBs in terms of cost and accessibility. A-deficient Na–Mn–O is one of the most competitive systems, in which various approaches were taken to enhance ARR, such as the substitution of electrochemical inactive species for TM; the extensive utilization of environmentally friendly elements, *e.g.*, Ti and Fe need further exploration. Although ARR offers attractive high capacity, challenges and uncertainties remain and overshadow the prospects. Irreversible lattice oxygen release and complex phase evolution are longstanding issues in the desodiation process of many ARR-based cathodes that induce capacity loss, voltage fading and hysteresis.[80] Modification strategies can bring some improvement. For instance, substitution (*e.g.*, Fe, Co) in the TM layer, doping of electrochemical inactive species or 4d/5d TM were reported to stabilize the struc-

ture and oxygen network;[66,81,82] surface coating with inactive compounds, *e.g.*, Al_2O_3, was reported to suppress lattice oxygen release related side reaction.[83] Except material design, innovative and ecomomical strategies should also be explored to develop high-energy-density NIB in technical aspects, *e.g.*, presodiation.[84,85] Beyond that, fundamentally understanding ARR is paramount. Therefore, developing advanced characterization methods is urgently needed, especially for *in-situ* and bulk studies; the 4d/5d TM-based cathodes are also significant model compounds to experimentally obtain a fundamental understanding.[19]

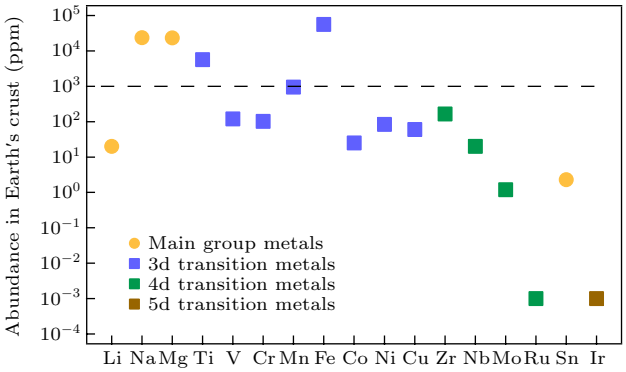


Fig. 6. Illustration of elemental abundance in the Earth crust; alkali metals (Li and Na), 3d, 4d, and 5d transition metals reported to comprise Li/Na-based cathodes are listed. The horizontal dashed line denotes 10^3 ppm.[79]

Acknowledgments

Project supported by the National Natural Science Foundation of China (Grant Nos. 51725206 and 52002394) and the Strategic Priority Research Program of the Chinese Academy of Sciences (Grant No. XDA21070500).

References

[1] Larcher D and Tarascon J M 2015 *Nat. Chem.* **7** 19
[2] Pan H, Hu Y S and Chen L 2013 *Energy Environ. Sci.* **6** 2338
[3] Hu Y S and Lu Y 2019 *ACS Energy Lett.* **4** 2689
[4] Li Y, Lu Y, Zhao C, Hu Y S, Titirici M M, Li H, Huang X and Chen L 2017 *Energy Storage Mater.* **7** 130
[5] Yin Y X, Yao H R and Guo Y G 2016 *Chin. Phys. B* **25** 018801
[6] Abraham K M 2020 *ACS Energy Lett.* **5** 3544
[7] Zhao C, Wang Q, Lu Y, Hu Y S, Li B and Chen L 2017 *J. Phys. D: Appl. Phys.* **50** 183001
[8] He S, Zhao J, Rong X, Xu C, Zhang Q, Shen X, Qi X, Li Y, Li X, Niu Y, Li X, Han S, Gu L, Liu H and Hu Y S 2022 *Chem. Eng. J.* **428** 131083
[9] Shen X, Zhou Q, Han M, Qi X, Li B, Zhang Q, Zhao J, Yang C, Liu H and Hu Y S 2021 *Nat. Commun.* **12** 2848
[10] Xu C, Zhao J, Wang E, Liu X, Shen X, Rong X, Zheng Q, Ren G, Zhang N, Liu X, Guo X, Yang C, Liu H, Zhong B and Hu Y S 2021 *Adv. Energy Mater.* **11** 2100729
[11] Shen X, Han M, Li X, Zhang P, Yang C, Liu H, Hu Y and Zhao J 2022 *ACS Appl. Mater. Interfaces* **14** 6841
[12] Guo G C, Wang C, Ming B M, Luo S W, Su H, Wang B Y, Zhang M, Yu H J and Wang R Z 2018 *Chin. Phys. B* **27** 118801
[13] Delmas C, Fouassier C and Hagenmuller P 1980 *Physica* **99B** 81
[14] Mu L Q, Hu Y S and Chen L Q 2015 *Chin. Phys. B* **24** 038202
[15] Ding Y, Ding F, Rong X, Lu Y and Hu Y S 2022 *Chin. Phys. B* **31** 068201
[16] Liu Q, Hu Z, Li W, Zou C, Jin H, Wang S, Chou S and Dou S X 2021 *Energy Environ. Sci.* **14** 158
[17] Ren H, Li Y, Ni Q, Bai Y, Zhao H and Wu C 2022 *Adv. Mater.* **34** 2106171
[18] Xu H, Guo S and Zhou H 2019 *J. Mater. Chem A* **7** 23662
[19] Assat G and Tarascon J M 2018 *Nat. Energy* **3** 373
[20] Robertson A D and Bruce P G 2003 *Chem. Mater.* **15** 1984
[21] Yu D Y W, Yanagida K, Kato Y and Nakamura H 2009 *J. Electrochem. Soc.* **156** A417
[22] Armstrong A R, Holzapfel M, Novák P, Johnson C S, Kang S H, Thackeray M M and Bruce P G 2006 *J. Am. Chem. Soc.* **128** 8694
[23] Seo D H, Lee J, Urban A, Malik R, Kang S and Ceder G 2016 *Nat. Chem.* **8** 692
[24] Aydinol M K, Kohan A F and Ceder G 1997 *Phys. Rev. B* **56** 1354
[25] Goodenough J B and Kim Y 2010 *Chem. Mater.* **22** 587
[26] Meng Y S, Ceder G, Grey C P, Yoon W S, Jiang M, Bréger J and Shao-Horn Y 2005 *Chem. Mater.* **17** 2386
[27] Luo K, Roberts M R, Hao R, Guerrini N, Pickup D M, Liu Y S, Edström K, Guo J, Chadwick A V, Duda L C and Bruce P G 2016 *Nat. Chem.* **8** 684
[28] Sauban'ere M, McCalla E, Tarascon J M and Doublet M L 2016 *Energy Environ. Sci.* **9** 984
[29] Yahia M B, Vergnet J, Sauban'ere M and Doublet M L 2019 *Nat. Mater.* **18** 496
[30] Okubo M and Yamada A 2017 *ACS Appl. Mater. Interfaces* **9** 36463
[31] Sudayama T, Uehara K, Mukai T, Asakura D, Shi X M, Tsuchimoto A, de Boisse B M, Shimada T, Watanabe E, Harada Y, Nakayama M, Okubo M and Yamada A 2020 *Energy Environ. Sci.* **13** 1492
[32] Tsuchimoto A, Shi X, Kawai K, de Boisse B M, Kikkawa J, Asakura D, Okubo M and Yamada A 2021 *Nat. Commun.* **12** 631
[33] Kitchaev D A, Vinckeviciute J and Van der Ven A 2021 *J. Am. Chem. Soc.* **143** 1908
[34] Song J H, Yoon G, Kim B, Eum D, Park H, Kim D H and Kang K 2020 *Adv. Energy Mater.* **10** 2001207
[35] Zhang K, Jiang Z, Ning F, Li B, Shang H, Song J, Zuo Y, Yang T, Feng G, Ai X and Xia D 2021 *Adv. Energy Mater.* **11** 2100892
[36] Zhao C, Wang Q, Yao Z, Wang J, Sánchez-Lengeling B, Ding F, Qi X, Lu Y, Bai X, Li B, Li H, Aspuru-Guzik A, Huang X, Delmas C, Wagemaker M, Chen L and Hu Y S 2020 *Science* **370** 708
[37] Maitra U, House R A, Somerville J W, Tapia-ruiz N, Lozano J G, Guerrini N, Hao R, Luo K, Jin L, Pérez-Osorio M A, Massel F, Pickup D M, Ramos S, Lu X, McNally D E, Chadwick A V, Giustino F, Schmitt T, Duda L C, Roberts M R and Bruce P G 2018 *Nat. Chem.* **10** 288
[38] Mu L, Xu S, Li Y, Hu Y S, Li H, Chen L and Huang X 2015 *Adv. Mater.* **27** 6928
[39] Mu L, Qi X, Hu Y, Li H, Chen L and Huang X 2016 *Energy Storage Sci. Technol.* **5** 324
[40] Li X, Bao J, Shadike Z, Wang Q, Yang X and Zhou Y 2021 *Angew. Chem. Int. Ed.* **60** 22026
[41] Rong X, Hu E, Lu Y, Meng F, Zhao C, Wang X, Zhang Q, Yu X, Gu L, Hu Y S, Li H, Huang X, Yang X, Delmas C and Chen L 2019 *Joule* **3** 503
[42] de la Llave E, Talaie E, Levi E, Nayak P K, Dixit M, Rao P T, Hartmann P, Chesneau F, Major D T, Greenstein M, Aurbach D and Nazar L F 2016 *Chem. Mater.* **28** 9064
[43] Xiao B, Liu X, Chen X, Lee G, Song M, Yang X, Omenya F, Reed D M, Sprenkle V, Ren Y, Sun C, Yang W, Amine K, Li X, Xu G and Li X 2021 *Adv. Mater.* **33** 2107141
[44] Ma X, Chen H and Ceder G 2011 *J. Electrochem. Soc.* **158** A1307
[45] Vassilaras P, Ma X, Li X and Ceder G 2013 *J. Electrochem. Soc.* **160** A207
[46] Yabuuchi N, Kajiyama M, Iwatate J, Nishikawa H, Hitomi S, Okuyama R, Usui R, Yamada Y and Komaba S 2012 *Nat. Mater.* **11** 512
[47] Yabuuchi N, Kubota K, Dahbi M and Komaba S 2014 *Chem. Rev.* **114** 11636
[48] Tamaru M, Wang X, Okubo M and Yamada A 2013 *Electrochem. Commun.* **33** 23
[49] de Boisse B M, Liu G, Ma J, Nishimura S I, Chung S C, Kiuchi H, Harada Y, Kikkawa J, Kobayashi Y, Okubo M and Yamada A 2016 *Nat. Commun.* **7** 11397
[50] Perez A J, Batuk D, Sauban'ere M, Rousse G, Foix D, McCalla E, Berg E J, Dugas R, van den Bos K H W, Doublet M, Gonbeau D, Abakumov A M, Van Tendeloo G and Tarascon J 2016 *Chem. Mater.* **28** 8278
[51] Rozier P, Sathiya M, Paulraj A, Foix D, Desaunay T, Taberna P, Simon P and Tarascon J 2015 *Electrochem. Commun.* **53** 29

[52] Zhang X, Qiao Y, Guo S, Jiang K, Xu S, Xu H Wang P, He P and Zhou H 2019 *Adv. Mater.* **31** 1807770

[53] Zhao C, Wang Q, Lu Y, Jiang L, Liu L, Yu X, Chen L, Li B and Hu Y S 2019 *Energy Storage Mater.* **20** 395

[54] Rong X, Gao F, Lu Y, Yang K ang Hu Y 2018 *Chin. Chem. Lett.* **29** 1791

[55] Zhang Y, Wu M, Ma J, Wei G, Ling Y, Zhang R and Huang Y 2020 *ACS Cent. Sci.* **6** 232

[56] Lu Z and Dahn J R 2001 *J. Electrochem. Soc.* **148** A1225

[57] Du K, Zhu J, Hu G, Gao H, Li Y and Goodenough J B 2016 *Energy Environ. Sci.* **9** 2575

[58] Adamczyk E and Pralong V 2017 *Chem. Mater.* **29** 4645

[59] Rong X, Liu J, Hu E, Liu Y, Wang Y, Wu J, Yu X, Page K, Hu Y S, Yang W, Li H, Yang X Q, Chen L and Huang X 2017 *Joule* **2** 125

[60] de Boisse B M, Nishimura S, Watanabe E, Lander L, Tsuchimoto A, Kikkawa J, Kobayashi E, Asakura D, Okubo M and Yamada A 2018 *Adv. Energy Mater.* **8** 1800409

[61] Dai K, Mao J, Zhuo Z, Feng Y, Mao W, Ai G, Pan F, Chuang Y, Liu G and Yang W 2020 *Nano Energy* **74** 104831

[62] Zhang J, Wang W, Wang W, Wang S and Li B 2019 *ACS Appl. Mater. Interfaces* **11** 22051

[63] House R A, Maitra U, Pérez-Osorio M A, Lozano J G, Jin L, Somerville J W, Duda L C, Nag A, Walters A, Zhou K J, Roberts M R and Bruce P G 2020 *Nature* **577** 502

[64] Gao A, Zhang Q, Li X, Shang T, Tang Z, Lu X, Luo Y, Ding J, Kan W H, Chen H, Yin W, Wang X, Xiao D, Su D, Li H, Rong X, Yu X, Yu Q, Meng F, Nan C, Delmas C, Chen L, Hu Y S and Gu L 2022 *Nat. Sustain.* **5** 214

[65] Huang Y, Zhu Y, Nie A, Fu H, Hu Z, Sun X, Haw S C, Chen J M, Chan T S, Yu S, Sun G, Jiang G, Han J, Luo W and Huang Y 2022 *Adv. Mater.* **34** 2105404

[66] Wang Q C, Meng J K, Yue X Y, Qiu Q Q, Song Y, Wu X J, Fu Z W, Xia Y Y, Shadike Z, Wu J, Yang X Q and Zhou Y N 2019 *J. Am. Chem. Soc.* **141** 840

[67] Li Y, Lu Y, Chen L and Hu Y S 2020 *Chin. Phys. B* **29** 048201

[68] Li X Y, Weng S T and Gu L 2020 *Chin. Phys. B* **29** 028801

[69] de Groot F M F, Grioni M and Fuggle J C 1989 *Phys. Rev. B* **40** 5715

[70] Roychoudhury S, Qiao R, Zhuo Z, Li Q, Lyu Y, Kim J, Liu J, Lee E, Polzin B J, Guo J, Yan S, Hu Y, Li H, Prendergast D and Yang W 2021 *Energy Environ. Mater.* **4** 246

[71] Boivin E, House R A, Pérez-Osorio M A, Marie J J, Maitra U, Rees G J and Bruce P G 2021 *Joule* **5** 1267

[72] Vergnet J, Saubanére M, Doublet M L and Tarascon J M 2020 *Joule* **4** 420

[73] Sathiya M, Leriche J B, Salager E, Gourier D, Tarascon J M and Vezin H 2015 *Nat. Commun.* **6** 6276

[74] Jia M, Li H, Qiao Y, Wang L, Cao X, Cabana J and Zhou H 2020 *ACS Appl. Mater. Interfaces* **12** 38249

[75] Shang T, Xiao D, Zhang Q, Wang X, Su D and Gu L 2021 *Chin. Phys. B* **30** 078202

[76] Fell C R, Qian D, Carroll K J, Chi M, Jones J L and Meng Y S 2013 *Chem. Mater.* **25** 1621

[77] Zhao E, Zhang Z G, Li X, He L, Yu X, Li H and Wang F 2020 *Chin. Phys. B* **29** 54

[78] Wang X, Tan S, Yang X Q and Hu E 2020 *Chin. Phys. B* **29** 028802

[79] Carmichael R S 1989 *Practical handbook of physical properties of rocks and minerals* (CRC Press)

[80] Eum D, Kim B, Song J H, Park H, Jang H Y, Kim S J, Cho S P, Lee M H, Heo J H, Park J, Ko Y, Park S K, Kim J, Oh K, Kim D H, Kang S J and Kang K 2022 *Nat. Mater.* **21** 664

[81] Zhao C, Yao Z, Wang J, Lu Y, Bai X, Aspuru-Guzik A, Chen L and Hu Y S 2019 *Chem.* **5** 2913

[82] Jiang L W, Lu Y X, Wang Y S, Liu L L, Qi X G, Zhao C L, Chen L Q and Hu Y S 2018 *Chin. Phys. Lett.* **35** 048801

[83] Liu Y, Fang X, Zhang A, Shen C, Liu Q, Enaya H A and Zhou C 2016 *Nano Energy* **27** 27

[84] Xie F, Lu Y, Chen L and Hu Y S 2021 *Chin. Phys. Lett.* **38** 118401

[85] Hu Y S and Li Y 2021 *ACS Energy Lett.* **6** 4115